Journal of
Translational Regenerative Medicine

2027. Volume 2

Research Paper

Gelatin-based Nanocomposite Scaffolds Containing Citrated Starch Nanoparticles for Sustained Delivery of Platelet-rich Plasma in Bone Tissue Engineering

Saeedeh Shokrolahi[1], Jhamak Nourmohammadi[1*], Seyyed Behnam Abdollahi Boraei[2], Ehsan Seyedjafari[3]

1. School of Life Science Engineering, College of Interdisciplinary Science and Technology, University of Tehran, Tehran, Iran.
2. Stem Cell and Regenerative Medicine Group, National Institute of Genetic Engineering and Biotechnology, Tehran, Iran.
3. Department of Biotechnology, College of Science, University of Tehran, Tehran, Iran.

Use your device to scan and read the article online

Citation Shokrolahi S, Nourmohammadi J, Abdollahi Boraei SB, Seyedjafari E. Gelatin-based Nanocomposite Scaffolds Containing Citrated Starch Nanoparticles for Sustained Delivery of Platelet-rich Plasma in Bone Tissue Engineering. Journal of Translational Regenerative Medicine. 2027; 2:e256240. http://dx.doi.org/10.22034/JTRM.2.1022

http://dx.doi.org/10.22034/JTRM.2.1022

ABSTRACT

Background: This study aimed to develop a multifunctional gelatin-based nanocomposite scaffold modified with citrated starch nanoparticles (CS-NPs) for the sustained delivery of platelet-rich plasma (PRP) in bone tissue engineering (BTE).

Methods: CS-NPs, with a primary particle size of 30–50 nm by TEM (number-weighted DLS peak at 36.2 nm) and a hydrodynamic Z-average of 691 nm (zeta potential: -2.21 mV), were prepared via nanoprecipitation and thermal esterification, loaded with PRP, and incorporated into a gelatin matrix to formulate three experimental groups: pristine gelatin (G), gelatin/CS-NPs (G-S), and PRP-loaded nanocomposite scaffolds (G-S-PRP).

Results: The fabricated scaffolds maintained interconnected pores (146–160 µm), high porosity (54–63%), and a compressive modulus ranging from 1.96 to 2.45 MPa. Release assessments showed an initial burst followed by sustained release of vascular endothelial growth factor (VEGF) and PDGF-BB over 21 days. In vitro culture with human adipose-derived mesenchymal stem cells demonstrated significantly enhanced cellular metabolic activity, extended cell morphology, ALP activity, and mineralization in the G-S-PRP group compared to the non-PRP controls.

Conclusion: Overall, the developed G-S-PRP scaffold provided an osteogenic-supportive microenvironment in vitro, demonstrating promising feasibility for low-load-bearing bone regeneration applications.

Keywords: Bone tissue engineering (BTE), Gelatin-based scaffolds, Citrated starch nanoparticles (CS-NPs), Platelet-rich plasma (PRP), Controlled release, Osteogenesis

Article info:
Received: 10 Nov 2026
Accepted: 22 Jan 2027
Publish: 02 Feb 2027

*** Corresponding Author:**
Jhamak Nourmohammadi, Associate Professor.
Address: *School of Life Science Engineering, College of Interdisciplinary Science and Technology, University of Tehran, Tehran, Iran.*
Phone: *+98 (21) 61115775*
E-mail: *J_nourmohammadi@ut.ac.ir*

Copyright © 2027 The Author(s);
This is an open access article distributed under the terms of the Creative Commons Attribution License (CC-By-NC: https://creativecommons.org/licenses/by-nc/4.0/legalcode.en), which permits use, distribution, and reproduction in any medium, provided the original work is properly cited and is not used for commercial purposes.

Highlights

- Multifunctional gelatin scaffolds integrated with citrated starch nanoparticles.
- Sustained release of VEGF and PDGF-BB was achieved over 21 days.
- PRP incorporation significantly enhanced hADMSC metabolic activity.
- Enhanced early osteogenesis with elevated ALP and calcium deposition.
- Developed a promising osteogenic nanocomposite for bone tissue engineering.

Plain Language Summary

Repairing damaged bone often requires biomaterials that physically support new tissue and steadily deliver healing signals. Platelet-rich plasma (PRP) contains vital growth factors that can accelerate bone regeneration, but these natural factors degrade rapidly when applied alone. In this study, we developed a sponge-like scaffold made of natural gelatin combined with citrated starch nanoparticles carrying PRP. This composite scaffold acts as a slow-release reservoir, steadily delivering the healing growth factors over a period of three weeks. When cultured with human stem cells in the laboratory, the scaffold promoted healthy cell growth and accelerated early mineral deposition essential for bone formation. These findings highlight a promising, natural nanobiocomposite scaffold that can provide a sustained healing microenvironment for bone tissue repair.

Introduction

The loss or dysfunction of bone tissue due to disease or trauma remains a significant challenge in modern healthcare. Although bone grafting is a gold-standard approach for treating skeletal defects, its clinical application is often hindered by limited graft availability, donor-site morbidity, potential pathogen transmission, and inconsistent long-term outcomes [1]. In this context, bone tissue engineering (BTE) has emerged as a promising strategy. Scaffolds play a pivotal role in BTE by mimicking the native extracellular matrix (ECM) and providing a supportive environment for cell adhesion, migration, proliferation, and differentiation. Furthermore, scaffolds can be integrated with carrier systems to enable the sequestration and controlled delivery of bioactive molecules [2].

Among various materials, natural biopolymers have gained considerable attention for scaffold fabrication due to their ECM-mimicking properties, biocompatibility, and ability to support cellular responses [3]. Gelatin, a collagen-derived polymer, is widely utilized as a scaffolding material and a delivery vehicle for bioactive molecules in BTE. Its inherent biocompatibility, low cost, and ease of processing, combined with the presence of bioactive motifs such as the arginine-glycine-aspartic acid (RGD) sequence, facilitate enhanced cell attachment and osteogenic activity [4]. Despite these advantages, many conventional scaffolds mainly serve as structural supports and lack the biological cues necessary to fully induce osteogenesis. While these scaffolds provide a surface for cell attachment, they often fail to effectively promote chemotaxis or regulate the synthesis of the native ECM [1, 2]. Consequently, developing multifunctional 3D scaffolds that combine structural integrity with the delivery of biochemical signals is a critical objective in this field [5].

Platelet-rich plasma (PRP) has emerged as a versatile, autologous source of essential growth factors, including platelet-derived growth factor (PDGF), transforming growth factor-β (TGF-β), vascular endothelial growth factor (VEGF), fibroblast growth factor (FGF), bone morphogenetic protein (BMP), and insulin-like growth factor (IGF). PRP provides a potent combination of growth factors that stimulate the osteogenic differentiation of mesenchymal stem cells [6]. However, the rapid, short-term release of these growth factors limits the clinical use of PRP by reducing its therapeutic window and biological efficacy [7]. Therefore, delivery systems that sustain the release of PRP-derived factors are urgently needed.

Polymeric nanocarriers are an effective strategy for controlled release of bioactive agents because of their high specific surface area and tunable surface chemistry. These nanocarriers can sequester growth factors within a scaffold's 3D network, preventing burst release without compromising structural stability [8]. Starch is a particularly attractive candidate for the fabrication of such nanocarriers due to its abundance, cost-effectiveness, and excellent biocompatibility [9]. Chemical modification of starch nanoparticles can significantly enhance their functionality for BTE applications [10]. Previous studies have demonstrated that negatively charged carriers are highly effective in the adsorption and sustained release of growth factors [11]. Specifically, modifying starch with citric acid introduces carboxyl groups, increasing negative surface charge density [12]. Thus, citrated starch nanoparticles (CS-NP) may serve as an effective nano vehicle for loading PRP and modulating the release profile of its bioactive components within a 3D scaffold.

In this study, starch nanoparticles were synthesized and modified with citric acid to produce negatively charged CS-NPs. These nanoparticles were loaded with PRP and incorporated into a gelatin-based scaffold to develop a bioactive nano-biocomposite system. We systematically evaluated the scaffolds' physicochemical properties, the release profiles of total protein and selected growth factors (VEGF and PDGF-BB), and cellular responses—including viability, proliferation, alkaline phosphatase (ALP) activity, and calcium deposition. This system is proposed as a preclinical model in biomaterials engineering for developing advanced bioactive platforms for bone regeneration.

Materials and Methods

Materials

Gelatin, citric acid, ethanol, polysorbate 80 (Tween 80), sodium hydroxide (NaOH), 1-ethyl-3-(3-dimethylaminopropyl) carbodiimide hydrochloride (EDC), and disodium hydrogen phosphate (Na_2HPO_4) were purchased from Sigma-Aldrich Company. Potato starch was obtained from BioBasic Company. For cell culture and osteogenic differentiation of human adipose-derived mesenchymal stem cells (hADMSCs) obtained from the Iranian Blood Transfusion Organization (IBTO, Tehran, Iran), Dulbecco's modified Eagle medium (DMEM), fetal bovine serum (FBS), and trypsin were purchased from Gibco Company. The 3-(4,5-dimethylthiazol-2-yl)-2,5-diphenyltetrazolium bromide (MTT) reagent, glutaraldehyde, dexamethasone, ascorbic acid, and penicillin-streptomycin were obtained from Sigma-Aldrich Company. VEGF and PDGF-BB ELISA kits were purchased from PeproTech Company, and alkaline phosphatase (ALP) and calcium assay kits were obtained from Pars Azmoon Company in Iran.

Synthesis of starch nanoparticles

Starch nanoparticles were prepared based on the method reported in our previous study [13], with slight modifications. First, a 0.27 M NaOH solution was prepared. Next, we prepared a 1.78% (w/v) starch solution by dissolving starch in the NaOH solution under heating and magnetic stirring for 1 h until a clear solution formed. Then, 0.32 mL of Tween 80, previously dissolved in 13 mL of distilled water, was added dropwise to the starch solution. Afterward, 70 mL of 99% ethanol was added under vigorous stirring to induce nanoparticle formation through nanoprecipitation. The resulting nanoparticles were collected by centrifugation at 11,000 rpm for 15 min and finally freeze-dried.

Surface modification of nanoparticles

To introduce carboxyl groups and functionalize the nanoparticles, we performed thermal esterification based on our previous study [12]. In this step, 1 g of starch nanoparticles was immersed in 10 mL of an ethanolic solution containing 3 g of citric acid. The suspension was stirred for 12 h to ensure complete diffusion of citric acid into the nanoparticle structure. Then, the ethanol was allowed to evaporate at room temperature. To complete the crosslinking and esterification reaction, the dried powder was heated at 120 ˚C for 1.5 h. After a visible color change, indicating completion of the reaction, the final product was milled and washed three times with deionized water to remove unreacted acid. Finally, CS-NPs were sonicated and dried at 50 ˚C. Transmission electron microscopy (TEM) was used to evaluate the morphology of the modified nanoparticles, while dynamic light scattering (DLS) and zeta potential analysis determined particle size and surface charge, respectively.

PRP preparation, activation, and loading procedure

PRP was prepared from standard blood donor units following certified clinical protocols. To activate the PRP and promote the release of bioactive growth factors, a cyclic freeze-thaw method was employed [14]. Briefly, under strict aseptic conditions, PRP was aliquoted into sterile microtubes and subjected to three consecutive freeze-thaw cycles consisting of freezing at -70 ˚C for 24

h followed by thawing in a water bath at 37 ˚C for 1 h. For PRP loading onto nanoparticles, an immersion technique was utilized. The CS-NPs were dispersed in activated PRP solution at a ratio of 100 mg of nanoparticles per 1.0 mL of PRP (100 mg/mL). The mixture was incubhdated at 4 ˚C for 1 h under gentle agitation (60 rpm) to facilitate protein adsorption. The loaded nanoparticles were subsequently frozen at -70 ˚C and lyophilized. The total mass of PRP immobilized onto the nanoparticles was gravimetrically quantified by determining the weight difference of independent samples (n=3) before and after loading, yielding an average loaded PRP content of approximately 13±1 mg.

Fabrication of gelatin-based scaffolds

A gelatin solution (3% w/v) was prepared by dissolving gelatin powder in distilled water at 37 ˚C under continuous stirring, and the solution was then allowed to cool first at room temperature. Starch nanoparticles were subsequently dispersed into the gelatin solution to achieve a final nanoparticle concentration of 3% w/v. We fabricated two scaffold formulations: the control scaffold, consisting of gelatin and unloaded starch nanoparticles (designated as G-S), and the PRP-loaded scaffold, consisting of gelatin and PRP-loaded starch nanoparticles (designated as G-S-PRP). The resulting mixtures were cast into 48-well plates, frozen at -70 ˚C and lyophilized to obtain porous scaffolds. To improve structural stability, the lyophilized scaffolds were crosslinked by immersion in an ethanol solution containing 20 mM EDC for 16 h at room temperature. After crosslinking, the scaffolds were thoroughly washed with 0.1 M sodium hydrogen phosphate solution to remove residual reagents, followed by a final lyophilization step.

Characterization of gelatin-based scaffolds

The morphology of the fabricated scaffolds was examined using a scanning electron microscopy (SEM) device (Model AIS2100, Seron Technology, South Korea). Scaffold cross-sections were analyzed at different magnifications after standard gold sputter-coating. To determine pore size and apparent sectional porosity, we obtained five randomly selected SEM images from each of three independent scaffold specimens per group (n=5) to ensure representative sampling. The images were analyzed in Image J software. The apparent sectional porosity was calculated using the following equation [15]: $A_p/A_T \times 100$, where A_p is the total area of the pores in the analyzed cross-section, and represents the total analyzed cross-sectional area. ImageJ software was used to measure both parameters and obtain the porosity.

The equilibrium water absorption capacity of the scaffolds was evaluated by immersing the samples in phosphate-buffered saline (PBS) for 24 h at 37 ˚C. Three specimens were analyzed for each group. The initial dry weight of each scaffold (W_0) was measured before immersion. After 24 h, the scaffolds were removed from the PBS, gently blotted to remove excess surface fluid, and weighed again (W_t). The equilibrium water absorption (g/g) was calculated using the Equation 1 [16]:

1. $W_t\text{-}W_0/W_0$

Where W_t was the weight of the swollen scaffold after the specified incubation period, and W_0 was the initial dry weight of the scaffold.

The mechanical behavior of hydrated scaffold discs (diameter: 6 mm, height-to-diameter ratio=2:1) evaluated by uniaxial compression testing in accordance with ASTM F451-86 guidelines using a universal testing machine (Zwick/Roell Z050) equipped with a 25 kN load cell. The scaffolds were compressed at a constant crosshead speed of 0.5 mm/min until exceeding 10% strain. The compressive modulus was calculated from the initial linear elastic slope of the stress-strain curve. The compressive strength was determined at 1% strain offset from the stress-strain curve. Tests were performed on three independent specimens per group and data are presented as Mean±SD [15].

The release of the selected growth factors VEGF and PDGF-BB from the PRP-loaded scaffolds was evaluated at predetermined time points. Three scaffold specimens, each weighing 5 mg, were transferred into sterile microtubes. Subsequently, 5 mL of PBS was added to each tube, and the samples were incubated at 37 ˚C. At 1, 4, 7, 14, and 21 days, 205 µL of the incubation medium was collected from each tube and stored at −70 ˚C until analysis. The removed volume was immediately replaced with an equal volume of fresh PBS to maintain a constant incubation volume.

The concentrations of VEGF and PDGF-BB in the scaffold extracts were determined using ELISA kits. First, 100 µL of the capture antibody solution was added to each well of a 96-well plate and incubated for 12 h. The wells were then washed with PBS, followed by adding 300 µL of blocking buffer. After a 2 h incubation, the wells were washed again. Next, 100 µL of each extract collected at the different time points was added to the appropriate wells and incubated for 2 h. After washing, 100 µL of avidin–horseradish peroxidase (avidin-HRP) conjugate was added to each well. The plate was incubated for

30 min and then washed to remove unbound conjugate. Subsequently, 100 µL of substrate solution was added to each well. The absorbance was measured at 450 nm for PDGF-BB and at 405 nm for VEGF using a microplate reader. The concentrations of VEGF and PDGF-BB were calculated based on the respective standard curves. The cumulative amounts of VEGF, and PDGF-BB were plotted as a function of incubation time using the mean values obtained from the experimental replicates.

Biological assessment

Isolation, seeding, and expansion of hADMSCs

The isolation of hADMSCs from subcutaneous adipose tissues of donor patients (aged 30–50 years) was conducted in accordance with the protocol used by Ataie et al. [16]. The harvested adipose specimens were minced, rinsed thoroughly using PBS, and enzymatically digested utilizing 0.02 mg/mL Collagenase type I (Sigma-Aldrich, Germany) under continuous agitation for 60 min at 37 ˚C. The digested mixture was centrifuged at 1000 rpm for 5 min to separate the stromal vascular fraction from the floating adipocytes. The resulting pellet was resuspended and transferred to culture flasks containing DMEM/F-12 (Gibco) supplemented with 10% FBS (Gibco), 100 U/mL penicillin (Gibco), 100 µg/mL streptomycin (Gibco), and 0.25 µg/mL amphotericin (Gibco). The primary cultures were maintained in a humidified incubator at 37 ˚C with 5%. The culture medium was replenished every 48 h until the monolayer reached approximately 80% confluence. For subsequent pre-clinical expansion, the cells were cultured in DMEM/F-12 supplemented with 10% FBS, 50 µg/mL ascorbic 2-phosphate (Sigma-Aldrich, Germany), 100 U/mL penicillin, and 100 µg/mL streptomycin. After reaching the target cell density at passage 4, hADMSCs were detached using a trypsin/EDTA solution (Gibco) for subsequent scaffold seeding.

Cell attachment and proliferation assays

Before cell seeding, the scaffolds were transferred to 24-well plates and disinfected by immersion in 70% ethanol for 20 min. The scaffolds were then rinsed three times with sterilized PBS to remove residual ethanol [15]. To evaluate initial cellular attachment, hADMSCs were seeded onto the fabricated scaffolds at a density of 2×10^4 cells/cm^2. Following a 7-day incubation period, the cell-scaffold constructs were fixed by immersion in a 2.5% (v/v) glutaraldehyde solution in PBS for 60 min. The fixed samples were then dehydrated through a graded series of ethanol solutions (increasing in 10% increments, 10 min per step). Finally, the dehydrated specimens were sputter-coated with gold prior to SEM imaging to visualize cellular morphology and integration.

Cell viability and metabolic activity were assessed using the MTT assay (Sigma, St. Louis, USA) [17]. The HADMSCs (2×10^4 cells/cm^2) were seeded onto sterilized scaffolds and incubated at 37 ˚C for 1, 4, and 7 days. At each time point, 50 µL of MTT stock solution (5 mg/mL) was added to each well, followed by incubation at 37 ˚C for 4 h. To solubilize the accumulated purple formazan crystals, 50 µL of dimethyl sulfoxide (Sigma) was introduced into each well and kept at room temperature for 10 min. The optical density (OD) of the dissolved formazan was measured at 570 nm using a microplate reader (ELISA Reader 96X; Convergys, Germany).

ALP activity assay

To assess early osteogenic differentiation, the enzymatic activity of ALP was quantified on days 7, 14, and 21 utilizing a commercial colorimetric assay kit (Pars Azmoon, Iran) [15]. Total intracellular protein was extracted by introducing RIPA lysis buffer to the cell-scaffold constructs, followed by centrifugation at 1500 rpm for 10 min at 4 ˚C to collect the supernatant. Subsequently, a 30 µL aliquot of the harvested supernatant was mixed with 1.4 mL of the working reagent (reagents 1 and 2 mixed at a 4:1 ratio according to the manufacturer's instructions). The mixture was incubated at 37 ˚C for 13 min. The resulting solution was transferred to a 96-well microplate, and the absorbance was measured spectrophotometrically at 405 nm using a microplate reader (ELISA-Reader 96X; Convergys, Germany). The enzymatic activity of ALP was normalized to the total protein content of each sample (U/mg protein).

Quantitative calcium deposition assay

The deposition of extracellular calcium mineral on the scaffolds was determined using a commercial calcium determination kit (Pars Azmoon, Iran) based on the cresolphthalein complexone method. Under alkaline conditions, free calcium ions react with cresolphthalein complexone to form a purple-colored coordination complex. The mineralized matrix on the scaffolds was dissolved by adding 3 N hydrochloric acid and the lysates were transferred to microtubes. A 6 µL volume of the dissolved sample was mixed with 1.3 mL of the kit reagent, followed by brief vortexing. The mixture was then transferred to a 96-well plate, and the OD was measured at 570 nm. The calcium concentration of each specimen was calculated against a standard curve.

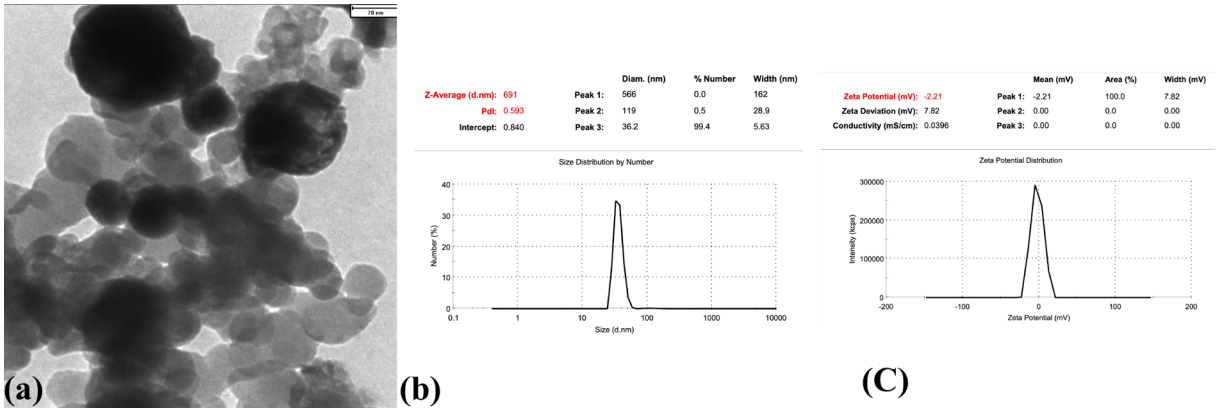


Figure 1. Characterization of the synthesized starch nanoparticles

a) TEM image, b) DLS size distribution, C) Zeta potential distribution

Statistical analysis

All experiments were conducted in triplicate and the experimental data were expressed as Mean±SD. For comparisons between two independent groups (e.g. physical, water-uptake, and mechanical properties), an independent Student's t-test was employed. For multi-group comparisons across multiple time points (e.g. MTT, growth factor release, ALP activity, and calcium deposition), two-way analysis of variance (ANOVA) followed by Tukey's post-hoc test was performed in GraphPad Prism (version 8.0, GraphPad Software, USA). Differences were considered statistically significant at $P<0.05$.

Results

Characterization of the nanoparticles

TEM analysis showed that the synthesized nanoparticles had a quasi-spherical morphology, with primary particle diameters of 30–50 nm (Figure 1a). DLS measurements showed an intensity-weighted hydrodynamic Z-average of 691 nm, whereas the number-weighted size distribution had a dominant peak at 36.2 nm (Figure 1b). The polydispersity index was 0.593. Moreover, zeta potential analysis showed a slightly negative surface potential of −2.21 mV (Figure 1c).

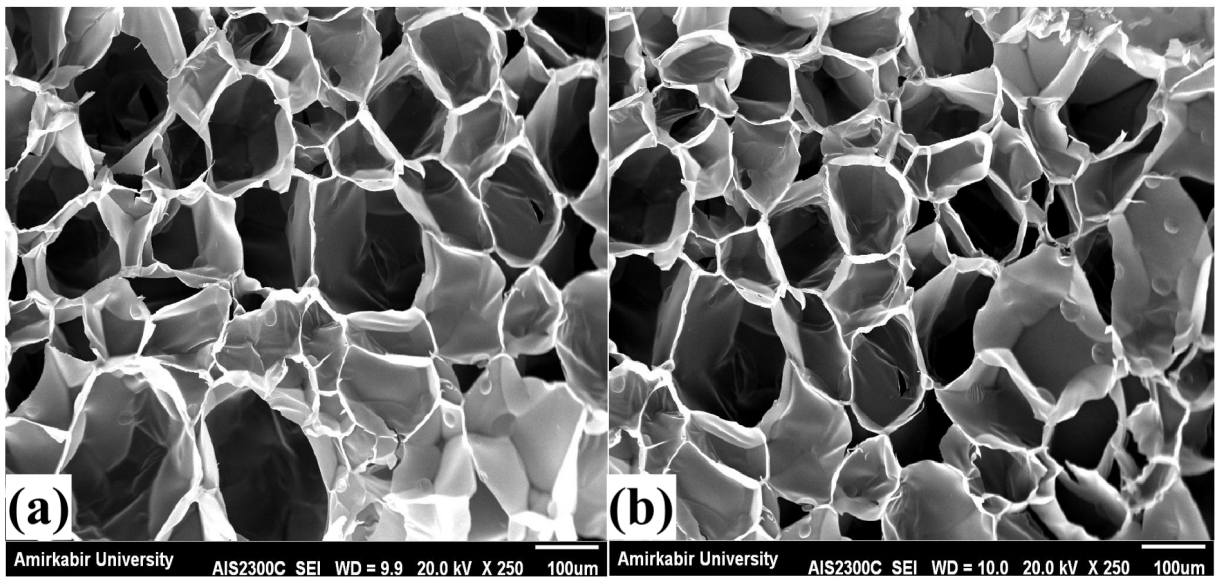


Figure 2. SEM images of the fabricated scaffolds

a) G-S, b) G-S-PRP

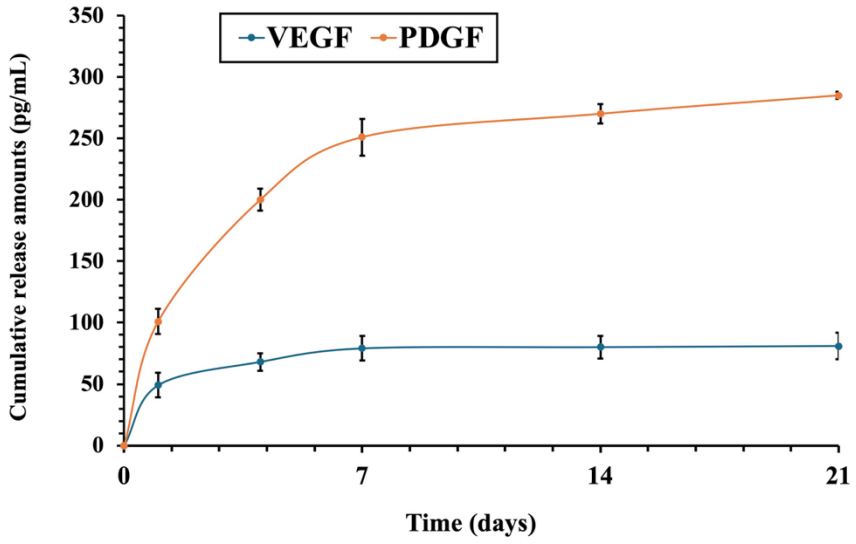


Figure 3. The cumulative release profiles of VEGF and PDGF from the scaffold over 21 days

Physical and mechanical properties

SEM images showed a porous architecture with interconnected pores in both G-S and G-S-PRP scaffolds (Figure 2). The mean pore diameters were 146±54 µm for G-S and 160±42 µm for G-S-PRP. Total porosity was 54±11% and 63±8%, respectively. No statistically significant differences in pore diameter or total porosity were reported between the two groups (P>0.05; Table 1). Equilibrium water uptake was 11.2±0.7 g/g for G-S and 12.4±0.4 g/g for G-S-PRP. The compressive modulus was 2.45±0.33 MPa and 1.96±0.21 MPa, respectively, and the compressive strength was 0.77±0.2 MPa and 0.71±0.1 MPa, respectively. We found no statistically significant differences between the two groups in water uptake, compressive modulus, or compressive strength. (P>0.05; Table 1).

Cumulative release profile

The cumulative release profiles of PDGF-BB and VEGF from G-S-PRP scaffolds were evaluated over 21 days, with sampling at 1 h, 4 h, 24 h, and days 3, 7, 14, and 21 (Figure 3). Both growth factors showed an initial burst within the first 24 h, followed by a slower, sustained release phase over the remainder of the evaluation period. PDGF-BB showed higher cumulative released concentrations than VEGF throughout the 21-day period.

Cell attachment and metabolic activity

SEM observations after 7 days of culture showed that HADMSCs attached to both scaffold surfaces (Figure 4). Cells on G-S-PRP appeared flatter, more spread, and more

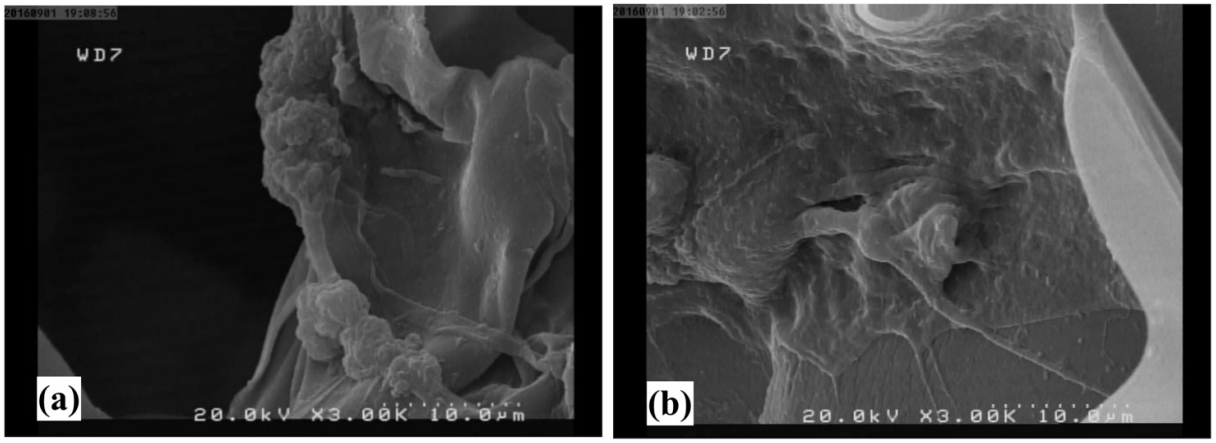


Figure 4. SEM images of the scaffolds seeded with hADMSCs after 7 days of in vitro culture

a) G-S, (b) G-S-PRP

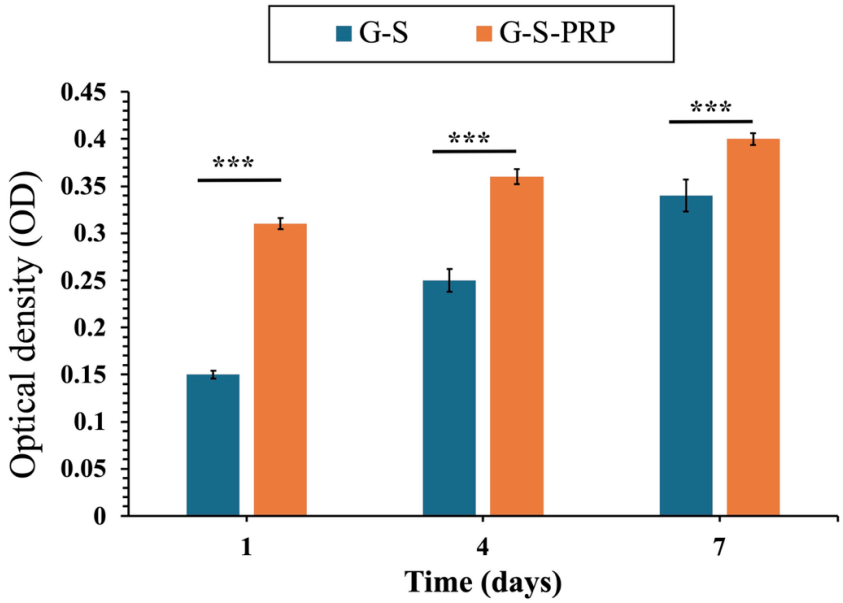


Figure 5. MTT assay of hADMSCs cultured on the different scaffolds at days 1, 4 and 7 following cell seeding

***P<0.001; The data are presented as Mean±SD.

widely distributed than those on G-S. The MTT assay showed a significantly higher cellular response on G-S-PRP than on G-S at days 1, 4, and 7 (Figure 5).

ALP activity and calcium deposition

ALP activity increased from day 7 to day 14 in both scaffold groups (Figure 6a). G-S-PRP showed higher ALP activity than G-S at days 7 and 14 (P<0.001 for both days). ALP activity reached its maximum at day 14 in both groups and decreased by day 21. At day 21, ALP activity was lower in G-S-PRP than in G-S (P<0.001). Calcium deposition increased over the 21-day culture period in both groups (Figure 6b). At day 14, calcium deposition was higher in G-S-PRP than in G-S; the figure indicated P < 0.01. At day 21, the reported calcium concentrations were approximately 3.5±0.05 mg/dL for G-S and 3.6±0.25 mg/dL for G-S-PRP. The final values were numerically similar, and no statistically significant difference was reported at day 21.

Discussion

The difference between the G-S and G-S-PRP scaffolds in the primary particle size measured by TEM and the intensity-weighted hydrodynamic size measured by DLS is consistent with colloidal aggregation in aqueous suspension. The number-weighted DLS peak was close

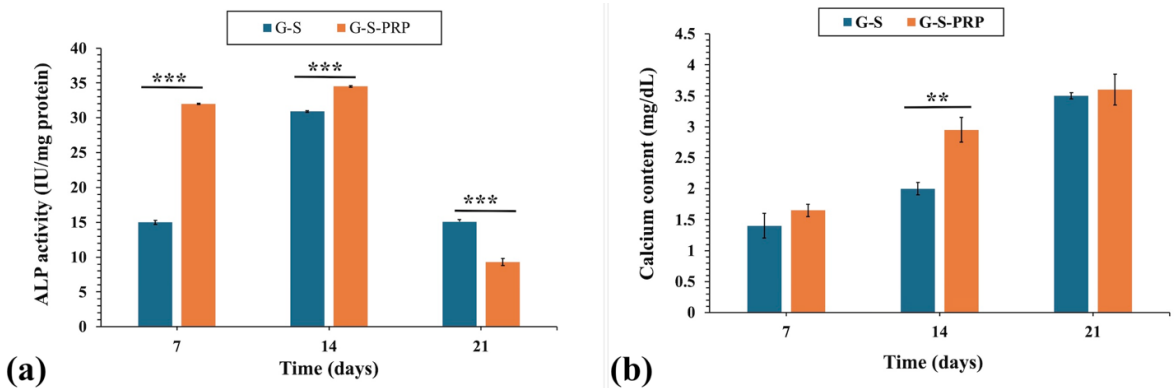


Figure 6. a) ALP activity, b) calcium content of hADMSCs seeded on G-S and G-S-PRP scaffolds after 7, 14, and 21 days of culture

**P<0.01, ***P<0.001.

Table 1. Physical and mechanical properties of the G-S and G-S-PRP scaffolds

Property	Mean±SD		P
	G-S	G-S-PRP	
Mean pore diameter (µm)	146±54	160±42	0.0321
Porosity (%)	54±11	63±8	0.0212
Equilibrium water uptake (g/g)	11.2±0.7	12.4±0.4	0.0442
Compressive modulus (MPa)	2.45±0.33	1.96±0.21	0.0238
Compressive strength (MPa)	0.77±0.2	0.71±0.1	0.0356

to the TEM particle-size range. Intensity-weighted DLS measurements are particularly sensitive to larger particles because scattering intensity increases strongly with particle diameter. Thus, a relatively small population of aggregates can substantially influence the Z-average.

The slightly negative zeta potential is consistent with citrate-derived carboxyl groups introduced onto the starch backbone, as discussed in relation to FTIR characterization [12]. The low magnitude of the measured potential suggests that electrostatic repulsion alone may not explain colloidal stability; steric stabilization by starch/citrate chains may also contribute. These interpretations should be distinguished from directly measured surface-charge and size data.

We selected PDGF-BB and VEGF because of their complementary roles in tissue repair. PDGF-BB participates in progenitor-cell recruitment, migration, and metabolic activation, whereas VEGF supports angiogenesis and early vascularization [18]. Their release profiles therefore provide relevant information about the PRP-loaded scaffold's delivery behavior.

The initial burst may reflect desorption and diffusion of loosely bound, surface-associated growth factors. The subsequent slower release may reflect diffusion of factors entrapped in, or interacting with, the citrated starch nanoparticle–gelatin matrix. This pattern could provide an early biochemical stimulus followed by continued availability of signaling molecules during culture. These release mechanisms are proposed interpretations rather than mechanisms directly established by the present experiments.

The higher cumulative concentration of PDGF-BB than VEGF may be related to differences in their initial abundance in activated PRP, consistent with the explanation proposed in a previous study [18]. Differences in molecular weight, isoelectric point, and interactions with carboxylated starch and the gelatin network may also influence release. Release measurements alone do not establish the biological activity of each released growth factor.

Pore size and interconnectivity influence cell migration, nutrient transport, and waste removal. Micro-pores can facilitate protein adsorption and initial cell attachment, while larger pores support tissue ingrowth and vascularization [15]. The observed interconnected architecture and pore sizes were therefore favorable structural features for further evaluation in bone tissue engineering.

The absence of statistically significant differences in pore size and porosity suggests that PRP incorporation did not produce a detectable change in the porous architecture under the tested conditions. Formation of the porous matrix through lyophilization and ice-crystal sublimation may help explain this preservation [15]. Maintaining pore architecture while incorporating biochemical cues could support cellular infiltration without disrupting the available physical space.

The high water uptake reported in our study is consistent with the hydrophilic nature of gelatin and starch [3, 4]. The similar water uptake of the two G-S and G-S-PRP samples also accords with their broadly preserved pore architecture. This swelling behavior may facilitate physiological fluid exchange, although the reported measurements did not directly establish fluid transport and blood infiltration [15].

Mechanical properties in porous scaffolds depend partly on porosity [19, 20]. Preservation of the porous structure may therefore help explain the lack of statistically significant differences in compression measurements after PRP loading. The measured compressive strengths (~0.7 MPa) fall well within the physiological range reported for low-density cancellous bone (0.1-5 MPa), including human mandibular trabecular bone (0.22-10.44 MPa) [21, 22]. This comparison suggests potential relevance to non-load-bearing or lightly loaded defects, including craniofacial and alveolar applications; it does not establish clinical load-bearing suitability.

Both G-S and G-S-PRP scaffolds supported cell attachment, while G-S-PRP showed a more extended cell morphology. Gelatin-derived RGD sequences may contribute to adhesion on G-S, and PRP-derived components may influence spreading on G-S-PRP. These observations are consistent with findings of Fukui et al. [22]. The morphology findings are qualitative and should not be interpreted as a quantitative measurement of adhesion strength.

The higher MTT response in G-S-PRP may be be due to the availability of PDGF and other PRP components. The initial release could contribute to the early cellular response, while continued release may support activity during subsequent culture. MTT primarily reflects cellular metabolic activity; it does not independently distinguish changes in cell number from changes in metabolism per cell. Nevertheless, the findings support favorable cytocompatibility under the reported in vitro conditions.

ALP activity and calcium deposition were evaluated as early and later indicators of osteogenic differentiation, respectively [17, 18]. ALP contributes to inorganic phosphate generation required for mineral formation [17, 18]. The higher ALP activity in G-S-PRP at days 7 and 14 supports an enhanced early osteogenic response. Both groups reached peak ALP activity at day 14; therefore, the data did not show an earlier peak ALP activity in G-S-PRP. The subsequent decline may be consistent with progression toward matrix maturation and mineralization, although this interpretation requires support from additional differentiation markers.

Higher calcium deposition in G-S-PRP at day 14 is consistent with the enhanced early osteogenic response. By day 21, however, the reported calcium concentrations were similar, indicating that the intermediate-stage advantage did not translate into a clearly demonstrated difference at the final time point. Santo et al. reported enhanced osteogenic differentiation of human adipose-derived stem cells in platelet-lysate-loaded 3D scaffolds [23]. Their reported earlier peak ALP activity and enhanced calcium detection provide related context, although platelet lysate and PRP are different preparations and the temporal profiles are not identical.

Taken together, the release and cell-culture findings suggest that the PRP-loaded scaffold provides an osteogenic-supportive microenvironment in vitro [6]. Proposed links between sustained growth factor release, cellular metabolic activity, and mineralization remain interpretive. These experiments alone cannot support clinical efficacy, in vivo vascularization, or performance in mechanically loaded defects.

Conclusion

We developed a gelatin-based nanocomposite scaffold incorporating CS-NPs for sustainable PRP delivery and evaluated it in vitro. The nanoparticles had a primary TEM size of 30–50 nm, a number-weighted DLS peak at 36.2 nm, a hydrodynamic Z-average of 691 nm, and a zeta potential of −2.21 mV. The PRP incorporation produced no statistically significant differences in the measured physical, swelling, or mechanical properties under the tested conditions. The G-S-PRP scaffold showed an earlier burst followed by sustained release of PDGF-BB and VEGF over 21 days. In hADMSC cultures, G-S-PRP supported greater cellular metabolic activity and a more extended cell morphology than G-S. ALP activity was higher in G-S-PRP at days 7 and 14, with both groups reaching their maximum at day 14. Calcium deposition was higher in G-S-PRP at day 14, while the reported values were similar at day 21. These findings support further investigation of the G-S-PRP scaffold as an osteogenic-supportive material in BTE; although its in-vivo performance and clinical suitability remain to be established.

Ethical Considerations

Compliance with ethical guidelines

All experimental protocols were in compliance with institutional biosafety guidelines for the use of human-derived biological products and internal laboratory safety standards.

Funding

This research did not receive any specific grant from funding agencies in the public, commercial, or not-for profit sectors.

Authors' contributions

Conceptualization, supervision, and funding administration: Jhamak Nourmohammadi; Methodology: Seyyed Behnam Abdollahi Boraei and Ehsan Seyedjafari; Experiments, data analysis, and writing the original draft: Saeedeh Shokrolahi; Data collection: Saeedeh Shokrolahi, Seyyed Behnam Abdollahi Boraei, and Ehsan Seyedjafari; Data analysis: Saeedeh Shokrolahi and Ehsan Seyedjafari; Data validation: Seyyed Behnam Abdollahi Boraei; Data interpretation: Ehsan Seyedjafari; Review and editing: Jhamak Nourmohammadi and Ehsan Seyedjafari; Final approval: All authors.

Conflict of interest

The authors declared no conflict of interest.

Acknowledgments

The authors gratefully acknowledge the Iranian Blood Transfusion Organization (IBTO) for kindly providing the human adipose-derived mesenchymal stem cells and PRP samples used in this research. Also, the authors would like to thank the research team at the University of Tehran for providing the necessary infrastructure and laboratory facilities to conduct this work.

References

[1] Sultana N. Bone tissue engineering: Scaffold design principles, biomaterial advances, and strategies for functional regeneration and clinical translation. Bioengineering. 2026; 13:514. [DOI:10.3390/bioengineering13050514] [PMID] [PMCID]

[2] Jang JW, Min KE, Kim C, Shin J, Lee J, Yi S. Review: Scaffold characteristics, fabrication methods, and biomaterials for the bone tissue engineering. International Journal of Precision Engineering and Manufacturing. 2023; 24:511-29. [DOI:10.1007/s12541-022-00755-7]

[3] Jo H, Kang S, Yang JE, Kim I, Lee SS. Biodegradable natural polymer-based drug delivery systems for bone tissue engineering. Medicinal Research Reviews. 2026; 46:966-88. [DOI:10.1002/med.70039] [PMID]

[4] Lukin I, Erezuma I, Maeso L, Zarate J, Desimone MF, Al-Tel TH, et al. Progress in gelatin as biomaterial for tissue engineering. Pharmaceutics, 2022; 14:1177. [DOI:10.3390/pharmaceutics14061177] [PMID] [PMCID]

[5] Bacevich BM, Smith RD, Reihl AM, Mazzocca AD, Hutchinson ID. Advances with platelet-rich plasma for bone healing. Biologics: Targets and therapy. Biologics. 2024; 18:29. [DOI:10.2147/BTT.S290341] [PMID] [PMCID]

[6] Yang J, Zheng L, Feng D, Song Y, Lei F. Immunomodulation and oxidative stress mitigation mediate enhanced bone regeneration by a platelet-rich plasma-loaded composite scaffold. Journal of Biomedical Materials Research Part B: Applied Biomaterials. 2026; 114:e70037. [DOI:10.1002/jbmb.70037] [PMID]

[7] Khandan-Nasab N, Torkamanzadeh B, Abbasi B, Mohajeri T, Oskuee RK, Sahebkar A. Application of platelet-rich plasma-based scaffolds in soft and hard tissue regeneration. Tissue Engineering Part B: Reviews. 2026; 32:245. [DOI:10.1089/ten.teb.2024.0285] [PMID]

[8] Hariawan BS, Miatmoko A, Anjani QK, Annuryanti F, Kamadjaja DB, Nurkanto A, et al. Nanomaterial application for protein delivery in bone regeneration therapy. Brazilian Journal of Medical and Biological Research. 2025; 58:e14057. [DOI:10.1590/1414-431x2024e14057] [PMID] [PMCID]

[9] Marta H, Rizki DI, Mardawati E, Djali M, Mohammad M, Cahyana Y. Starch nanoparticles: Preparation, properties and applications. Polymers. 2023; 15:1167. [DOI:10.3390/polym15051167] [PMID] [PMCID]

[10] Araújo RN, Bitencourt BS, de Aguiar SB, Sponchiado PA, Kirsten PN, Tessaro L, et al. Recent advances on starch-based biomaterials: A review. ACS Polymers Au. 2026; 6:520-34. [DOI:10.1021/acspolymersau.5c00188] [PMID] [PMCID]

[11] Wu D, Eugenis I, Hu C, Kim S, Kanugovi A, Yue S, Wheeler JR, et al. Bioinstructive scaffolds enhance stem cell engraftment for functional tissue regeneration. Nature Materials. 2025; 24:1364-74. [DOI:10.1038/s41563-025-02212-y] [PMID] [PMCID]

[12] Nourmohammadi J, Amoabediny G. Biomimetic formation of calcium phosphate on the citrated-starch suitable for bone tissue engineering. Starch. 2016; 68:1275-81. [DOI:10.1002/star.201500216]

[13] Davari N, Nourmohammadi J, Mohammadi J. Nitric oxide-releasing thiolated starch nanoparticles embedded in gelatin sponges for wound dressing applications. International Journal of Biological Macromolecules. 2024; 265:131062. [DOI:10.1016/j.ijbiomac.2024.131062] [PMID]

[14] Moaddab M, Nourmohammadi J, Rezayan AH. Bioactive composite scaffolds of carboxymethyl chitosan-silk fibroin containing chitosan nanoparticles for sustained release of ascorbic acid. European Polymer Journal. 2018; 103:40. [DOI:10.1016/j.eurpolymj.2018.03.032]

[15] Mashhadi R, Nourmohammadi J, Tavakol M. Enzymatically crosslinked pectin-silk fibroin hydrogel with embedded ZnO@Gallic acid nanoparticles: An injectable, self-healing, and antibacterial wound dressing. International Journal of Biological Macromolecules. 2026; 17(349):150823. [DOI:10.1016/j.ijbiomac.2026.150823] [PMID]

[16] Ataie M, Nourmohammadi J, Seyedjafari E. Carboxymethyl carrageenan immobilized on 3D-printed polycaprolactone scaffold for the adsorption of calcium phosphate/strontium phosphate adapted to bone regeneration. International Journal of Biological Macromolecules. 2022; 206:861-874. [DOI:10.1016/j.ijbiomac.2022.03.096] [PMID]

[17] Tang L, Cai S, Lu X, Wu D, Zhang Y, Li X, et al. Platelet-derived growth factor nanocapsules with tunable controlled release for chronic wound healing. Small. 2024; 20:2310743. [DOI:10.1002/smll.202310743] [PMID]

[18] Nourmohammadi J, Roshanfar F, Farokhi M, Haghbin Nazarpak M. Silk fibroin/kappa-carrageenan composite scaffolds with enhanced biomimetic mineralization for bone regeneration applications. Materials Science and Engineering. 2017; 76:951-958. [DOI:10.1016/j.msec.2017.03.166] [PMID]

[19] Bignon A, Chouteau J, Chevalier J, Fantozzi G, Carret JP, Chavassieux P, et al. Effect of micro- and macroporosity of bone substitutes on their mechanical properties and cellular response. Journal of Materials Science: Materials in Medicine. 2003; 14(12):1089-97. [DOI:10.1023/B:JMSM.0000004006.90399.b4] [PMID]

[20] Misch CE, Qu Z, Bidez MW. Mechanical properties of trabecular bone in the human mandible: implications for dental implant treatment planning and surgical placement. Journal of Oral and Maxillofacial Surgery. 1999; 57(6):700-6; discussion 706-8. [DOI:10.1016/S0278-2391(99)90437-8] [PMID]

[21] Morgan EF, Unnikrisnan GU, Hussein AI. Bone mechanical properties in healthy and diseased states. Annual Review of Biomedical Engineering. 2018; 20:119-43. [DOI:10.1146/annurev-bioeng-062117-121139] [PMID] [PMCID]

[22] Fukui M, Lai F, Hihara M, Mitsui T, Matsuoka Y, Sun Z, et al. Activation of cell adhesion and migration is an early event of platelet-rich plasma (PRP)-dependent stimulation of human adipose-derived stem/stromal cells. Human Cell. 2024; 37:181. [DOI:10.1007/s13577-023-00989-1] [PMID]

[23] Santo VE, Duarte AR, Popa EG, Gomes ME, Mano JF, Reis RL. Enhancement of osteogenic differentiation of human adipose derived stem cells by the controlled release of platelet lysates from hybrid scaffolds produced by supercritical fluid foaming. Journal of Controlled Release. 2012; 162:19. [DOI:10.1016/j.jconrel.2012.06.001] [PMID]